Understanding the biological context of NS5A-host interactions in HCV infection- a network based approach

Lokesh P. Tripathi[1¶]*, Hiroto Kambara[2¶], Yi-An Chen[1], Yorihiro Nishimura[2], Kohji Moriishi[2], Toru Okamoto[2], Eiji Morita[2], Takayuki Abe[2], Yoshio Mori[2], Yoshiharu Matsuura[2], Kenji Mizuguchi[1,3]*

[1]National Institute of Biomedical Innovation, 7-6-8 Saito Asagi, Ibaraki, Osaka, 567-0085, Japan.

[2]Department of Molecular Virology, Research Institute for Microbial Diseases, Osaka University, 3-1 Yamada-Oka, Suita, Osaka, 565-0871, Japan.

[3]Graduate School of Frontier Biosciences, Osaka University, 1-3 Yamada-Oka, Suita, Osaka, 565-0871, Japan

[¶]These authors contributed equally to this work.

*Correspondence should be addressed to Kenji Mizuguchi, National Institute of Biomedical Innovation, 7-6-8 Saito Asagi, Ibaraki, Osaka 567-0085, Japan. E-mail: kenji@nibio.go.jp; Tel: +81-72-641-9890; Fax: +81-72-641-9881 or to Lokesh P. Tripathi at lokesh@nibio.go.jp.

Supplementary text

Materials and Methods

Yeast two-hybrid protein assay-selection of positive clones

Since the bait constructs may sometimes self-transactivate the reporter genes, the N5SA-containing bait plasmid was tested for auto-activation, whereby the NS5A-Gal4-DB bait plasmid and an empty prey plasmid were co-transfected into the AH109 yeast strain and subjected to a beta-galactosidase assay according to the method of Duttweiler [1]. We confirmed that the NS5A-containing bait did not exhibit auto-transcriptional activation in the drop-out media that are deficient in Ade, His, Leu and Trp (Figure S1).

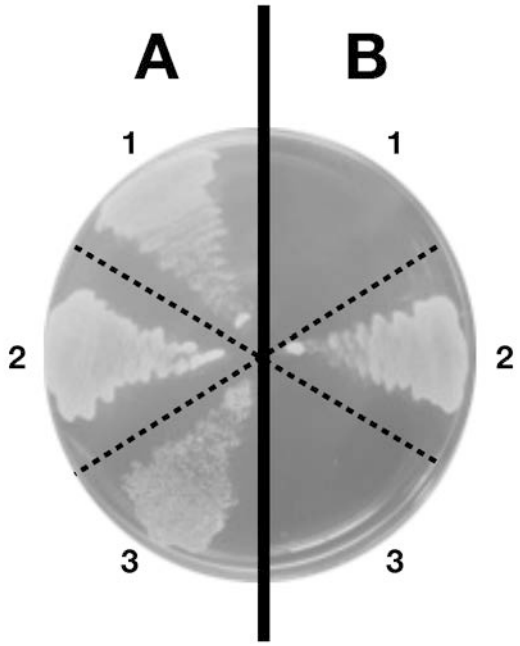

Supplementary Figure S1: NS5A does not exhibit auto-activation in a yeast two-hybrid assay. A pair of empty bait and prey plasmids as negative control (1), p53 (bait) and Large T (prey) as positive control (2) and NS5A-containing bait and an empty prey plasmid (3), were introduced into the AH109 yeast strain. Each yeast clone including the bait and prey

plasmids was inoculated on drop-out plates lacking Leu and Trp (A), or Leu, Trp, His, and Ade (B), and then incubated at 30˚C for 2 days.

The primary positive clones were first selected on the drop-out media that are deficient in Ade, His, Leu and Trp. Yeast colonies grown on the dropout plates lacking Ade, His, Leu, and Trp and were reinoculated on two fresh dropout plates lacking Trp, Leu, His and Ade, for confirmation. The resulting clones were then inoculated on two new dropout plates lacking Leu and Trp. One of the two Leu-/Trp-dropout plates was subjected to a beta-galactosidase assay, and the other plate was stored at 4ºC as the master plate. The positive prey plasmids were isolated from the master plate corresponding to each beta-gal-positive yeast clone and were retested in a fresh AH109 yeast strain by co-transfecting with the NS5A containing bait plasmid. The total DNA was isolated from each colony of the master plate corresponding to each beta-gal-positive yeast clone and then transfected into a competent *E. coli* strain JM109. The prey plasmid was recovered from the bacterial colonies grown on a plate containing ampicillin. The insert sequence of each purified plasmid was determined by using the Big Dye terminator reaction mixture and the ABI Prism 310 genetic analyzer (Applied Biosystems) and was searched against the NCBI NR database to obtain the corresponding transcript sequences. Each positive prey plasmid was transfected into the AH109 yeast strain together with an empty bait plasmid and the resulting clone was tested for auto-activation using the beta-galactosidase assay. Seventeen positive clones were identified in this manner (Table S1).

Supplementary Table S1: Y2H assay identified 17 cDNA clones encoding NS5A interacting proteins

Gene ID	**Symbol**	**Nucleotide Accession No.**	**Description**	**ORF**	**Frame**
23204	ARL6IP1	NM_015161.1	ADP-ribosylation factor-like 6 interacting protein 1	Full length	In frame

4508	ATP6	AAB58948.1	ATP synthase F0 subunit 6	Partial	In frame
274	BIN1	NM_139344.2	bridging integrator 1	Partial	In frame
89927	C16orf45	BC023603.2	chromosome 16 open reading frame 45	Partial	In frame
2051	EPHB6	NM_004445.3	EPH receptor B6	Partial	In frame
23770	FKBP8	NM_012181.3	FK506 binding protein 8, 38kDa	Full length	In frame
11345	GABARAPL2	NM_007285.6	GABA(A) receptor-associated protein-like 2	Partial	In frame
6453	ITSN1	NM_001001132.1	intersectin 1	Partial	In frame
9448	MAP4K4	NM_145687.3	mitogen-activated protein kinase kinase kinase kinase 4	Partial	In frame
11188	NISCH	NM_007184.3	nischarin	Partial	In frame
6167	RPL37	NM_000997.4	ribosomal protein L37	Full length	In frame
6252	RTN1	NM_206852.2	reticulon 1	Partial	In frame
10313	RTN3	NM_006054.3	reticulon 3	Partial	In frame
25777	SUN2	AF202723.1	Sad1 and UNC84 domain containing 2	Partial	In frame
9217	VAPB	NM_004738.4	VAMP (vesicle-associated membrane protein)-associated protein B and C	Full length	In frame
10493	VAT1	NM_006373.3	vesicle amine transport protein 1 homolog (T. californica)	Partial	In frame
9726	ZFP28	NM_014699.3	zinc finger protein 28 homolog (mouse)	Partial	In frame

Gene/Protein/EST Expression analysis

The 132 NS5A interactors (and the components of the NS5A infection network) were surveyed for the corresponding gene expression in the liver (including hepatocellular carcinoma and hepatic cells with and without HCV infection) by using EBI Gene expression atlas (GXA) [2]; MacPherson et al. [3] or NCBI dbEST [4] datasets (Table S3). The protein expression of the 132 primary NS5A interactors in liver tissue and liver cancer was also investigated by using the Human Protein Atlas [5] (Table S3).

Generation of High-confidence Human PPI network

To minimise the number of false positives, only high-confidence PPIs supported by at least two different experimental methods or two independent publications were subsequently retained from the unfiltered Human PPI network. Furthermore, only the high-confidence PPIs that were tagged as direct physical interactions by the iRefindex curators and/or identified as

direct physical interactions by at least one supporting experimental procedure (such as Y2H, fluorescence energy resonance transfer, atomic force microscopy [6]) and/or the supporting PMIDs were retained. The resulting human PPI network is composed of 22,789 PPIs involving 7,648 human proteins. We further extracted the largest connected component of the above human PPI network by removing smaller clusters and isolated nodes to infer a high-confidence human protein interactome (HPI) comprising 22,532 non-redundant binary physical interactions between 7,277 proteins (Figure S2; Table S5b). Of the 22,532 interactions in the HPI, 10,461 (46.4%) were supported by one or more MI terms (such as MI:0225; MI:0946; MI:1087; MI:0411; MI:0047; MI:0678; MI:0695; MI:0095; MI:0004; MI:0019; MI:0006; MI:0007; MI:0402; MI:0225; MI:1218; MI:1028; MI:1029; MI:0858; MI:0946; MI:1017 and MI:0729), which were judged to describe immunoaffinity-based experimental methods to detect protein-protein interactions. Likewise, 152 of 22,532 interactions in the HPI (0.67%) were supported by one or more MI terms (such as MI:0943; MI:0069; MI:1246; MI:1238; MI:0944 and MI:0676), which were judged to describe mass spectrometry-based experimental methods to detect protein-protein interactions.

HPI was subsequently used to identify biologically relevant trends, the significance of which was assessed by using randomised networks.

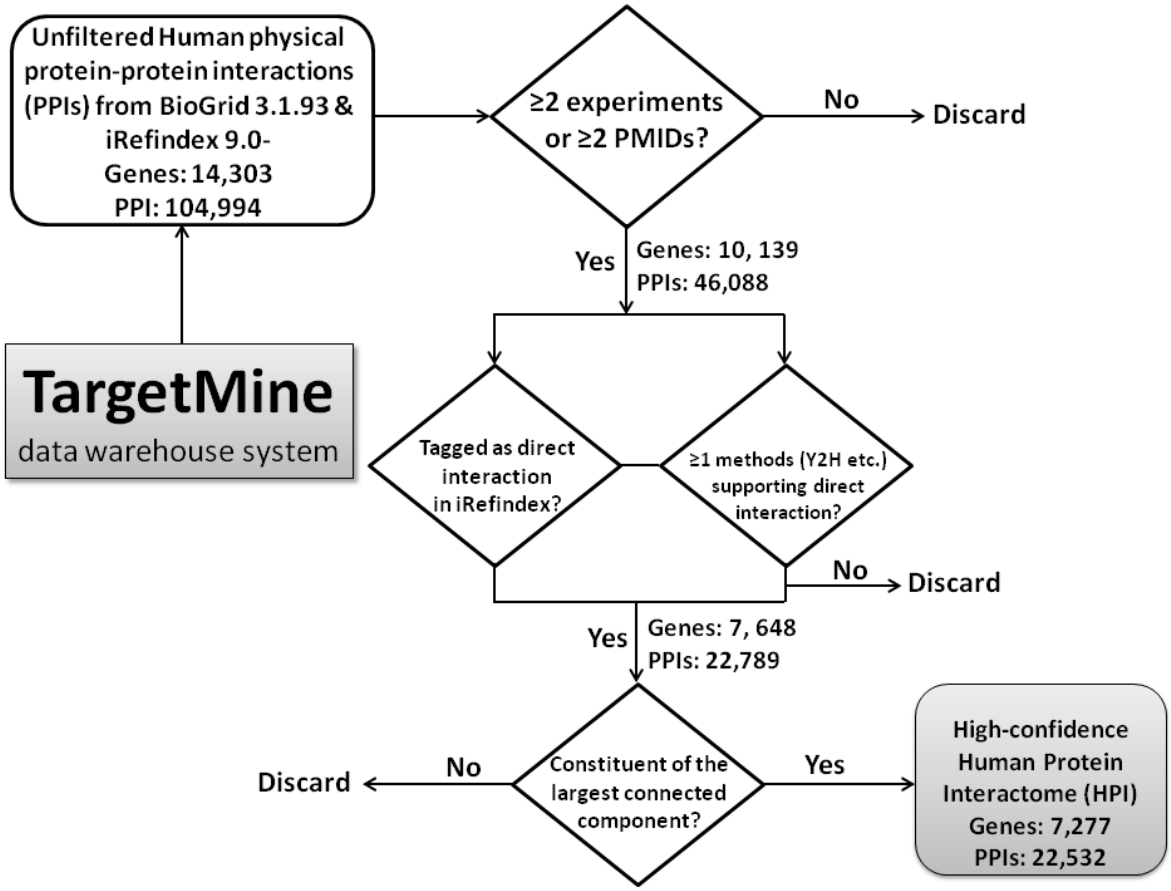

Supplementary Figure S2: Flowchart showing the construction of HPI by extracting high confidence direct physical human PPIs from BioGrid 3.1.93 and iRefindex 9.0 repositories using TargetMine.

Degree-preserved network randomisation tests

To compare the characteristics of HPI with those of random networks, 1000 randomly connected networks with identical degree distributions to HPI were generated using the RandomNetworks plugin in Cytoscape. Degree preserving networks were created by shuffling the original network by randomly choosing an existing pair of edges in the original HPI and rewiring them. The number of rewiring steps taken was 225320 (10× the number of edges in HPI), involving 21827 edges in the HPI. The distance between the observed values and the simulated values was normalised using a *Z*-score, which is defined as $Z=x-\mu/\sigma$, where

x is the observed value, μ is the mean of the simulated values, and σ is the standard deviation of the simulated values.

To test if NS5A had a proclivity to target well connected nodes (hubs) and bottlenecks in the HPI, we randomly selected a group of 108 nodes (the same number of nodes as targeted by NS5A in HPI) from the HPI and computed their average degrees and determined the fraction of bottlenecks in HPI amongst them. This procedure was repeated 1000 times. We defined the *p*-value of the significance of these two observations (hubs and bottlenecks) using the fraction of the average node degrees or bottlenecks under simulated conditions that was greater than the actual average degree for the NS5A-targeted nodes.

Results

Literature mining for pairwise NS5A-human interactions

Twenty two pairwise interactions between NS5A and human proteins were extracted from various literature reports as summarised in Table S2.

Supplementary Table S2: List of pairwise NS5A-host protein interactions extracted from various publications using a text mining approach combined with manual curation.

Gene ID	Symbol	Interaction detection method	Evidence of direct interaction discerned from author statement	PMID
60	ACTB	Coimmunoprecipitation	HCV NS3 and NS5A directly interact with tubulin and actin	18562541
10598	AHSA1	Yeast two-hybrid system (Y2H)		17616579
302	ANXA2	Coimmunoprecipitation	Anxa2 specifically coprecipitated NS3/NS4A, NS4B, NS5A, and NS5BΔTM but not core, E1E2, NS3, or GST protein	22301157
1452	CSNK1A1	*In vitro* kinase assay	NS5A is directly phosphorylated by CKI-α	17166835
1457	CSNK2A1	*In vitro* kinase assay	CKII could be the main protein kinase responsible for basal NS5A phosphorylation; Serine 457 is a phosphoacceptor site, and that this site is a target of CKII	19073181; 18369478

1499	CTNNB1	Coimmunoprecipitation; Immunoprecipitation; Immunoblot	NS5A is able to bind to both β-catenin and the p85 subunit of PI3K	19846673; 19726098
2316	FLNA	Immunoprecipitation	Co-IP using anti-fila antibody followed by the detection of HCV proteins' immunoreactive band further confirmed that fila directly interacts with NS3 and NS5A proteins	21914078
8880	FUBP1	Coimmunoprecipitation	FBP may modulate HCV replication by interacting with viral protein NS5A in the cells	18400844
3303	HSPA1A	Tandem affinity purification; Coimmunoprecipitation	Identification of HSC70 and Hsp72 as cellular targets interacting with NS5A	20601427
3315	HSPB1	Coimmunoprecipitation	The N-region of NS5A specifically interacts with the N-terminal half of HSP27	15120631
4256	MGP	Yeast two-hybrid system (Y2H); GST pulldown		15607035
5007	OSBP	Immunoprecipitation	NS5A interacts with OSBP	19570870
5295	PIK3R1	GST pulldown; Coimmunoprecipitation	NS5A directly interacts with the p85 subunit of PI3K, which, in turn, mediates the NS5A-Gab1 association	12186904; 19846673
5300	PIN1	*In vitro* GST pulldown; Coimmunoprecipitation; Immunoprecipitation	Pin1 interacts directly with both the HCV NS5A and NS5B proteins	21680504
5347	PLK1	Coimmunoprecipitation; *In vitro* kinase assay	Direct interaction and colocalization between Plk1 and NS5A	20534861
5478	PPIA	Mammalian two-hybrid; AlphaLISA		20132841
5515	PPP2CA	GST pulldown; Coimmunoprecipitation	NS5A protein interacts *in vivo* and *in vitro* with the scaffolding A and the catalytic C subunits of PP2A	16460864
5518	PPP2R1A	GST pulldown; Coimmunoprecipitation	NS5A protein interacts *in vivo* and *in vitro* with the scaffolding A and the catalytic C subunits of PP2A	16460864
91543	RSAD2	Confocal microscopy and Fluorescence resonance energy transfer (FRET) analysis	Viperin is able to interact with core and NS5A on the LD surface and with NS5A within the RC	22045669
284297	SSC5D	Yeast two-hybrid system (Y2H); GST pulldown		15607035
6772	STAT1	Immunoprecipitation	[D]ata suggest a direct physical interaction between the NS5A and STAT1 proteins	19570870
6850	SYK	Coimmunoprecipitation; *In vitro* kinase assay	NS5A interacts specifically with Syk	18420802

Overlapping probabilities between Y2H screening and the combined literature dataset

Using a Y2H assay, we identified 17 host factors as interacting partners of NS5A, 13 of which are novel. The other three interactions (BIN1, FKBP8 and VAPB) have been characterised previously. We then scanned the literature for additional NS5A intearctors. A study by de Chassey *et al*., reported 95 unique interactors of NS5A [7]; since two host factors in their dataset (BIN1 and VAPB) were also identified by our Y2H assay, 93 IPs from the de Chassey dataset were included in our analysis. We further extracted 22 IPs from the literature that were not included in the above two datasets (Table S2), giving us a total of 132 NS5A interacting host proteins.

The small overlap between the PPIs identified in our approach and the de Chassey dataset is not inconsistent with the small overlap in general between Y2H screens investigating host-viral interactions [8] and high false-negative rates associated with proteome-wide Y2H screens [9]. Furthermore, de Chassey *et al*. hypothesised that different methods of screening may lead to the exploration of different spaces of the HCV-human interactome.

To investigate if the observed overlap (m=3) between NS5A interactors identified in our study ($n1$=17) and known NS5A interactors from the literature ($n2$=118) was statistically significant, we employed the approach of Fury *et al*., [10]. As per this approach, if two gene lists containing $n1$ and $n2$ genes, respectively, are sampled from a larger set of n genes (here we used 22,496, the number of genes expressed in the liver as per GXA as an estimate of this number), the probability that the two lists will have m genes in common is the hypergeometric distribution. The probability of overlap was calculated using the Fisher's exact test in R with the following 2-by-2 table:

3	14
115	22364

The *p*-value for the overlap was 9.067×10^{-5}, suggesting that the overlap between NS5A interactors identified by our Y2H and previously known interactions was statistically significant.

HPI has significantly shorter average shortest path length compared with degree-preserved randomised PPI networks.

We compared the average shortest path length (APL) of HPI with those of the randomised PPI networks. The observed APL of the HPI (4.54) was much higher than the mean APL of the randomised networks (4.13±0.007) (Figure S3). The *Z*-score of this observation was 52.77 and the *p*-value for the significance of this observation was <0.001. Our results are consistent with a previous study that real world PPI networks have longer path lengths than randomly rewired connected networks with identical degree distributions [11].

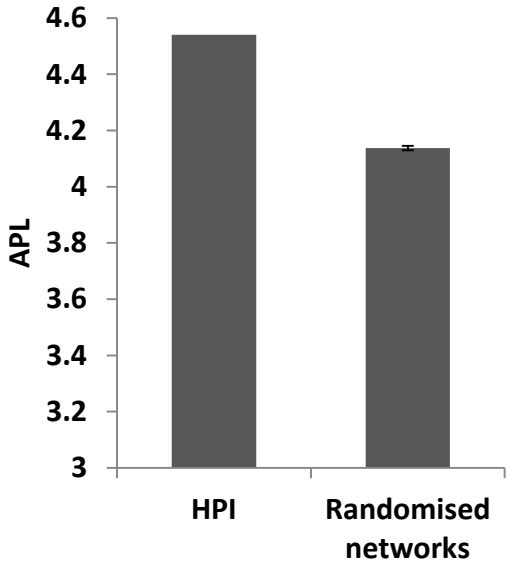

Supplementary Figure S3: The average shortest path length (APL) of the HPI is much higher than the mean APL of 1000 degree-preserved randomised PPI networks.

NS5A selectively targets hubs and bottlenecks in HPI

We compared the average degree of the 108 nodes targeted by NS5A in the HPI with the mean average degree of 1000 sets of randomly selected nodes. The average degree of the NS5A-targeted nodes in the HPI (19.02) was significantly higher than the mean average degree of the randomly selected nodes (6.17±1.08) (Figure 1B) and was even higher than the maximum average degree observed for the randomly selected nodes (12.59) from 1,000 simulations; the *p*-value for the significance of this observation is <0.001.

We next compared the fraction of bottlenecks amongst the 108 nodes targeted by NS5A in the HPI with those of 1000 sets of randomly selected nodes. Thirty-nine NS5A interactors were identified as bottlenecks in the HPI, which was significantly higher than the mean of the number of bottlenecks amongst the randomly selected nodes (10.72±3.17) (Figure 1D) and was even higher than the maximum number of bottlenecks observed for a set of randomly selected nodes (21); the *p*-value for the significance of this observation is also <0.001.

Our observations thereby suggest that NS5A preferentially targets hubs and bottlenecks in the host protein interactome.

Functional analysis of NS5A interaction network

Development

In the NS5A infection network, 13 bottlenecks were mapped to various enriched pathways associated with Development (Table S7a). Eleven bottlenecks were mapped to the enriched KEGG pathway "Osteoclast differentiation" ($p=1.02\times10^{-17}$), which is consistent with descriptions of Hepatitis C-induced osteosclerosis (HCAO) in HCV-infected patients [12]. Our observations suggest that NS5A may play an important role in HCAO in HCV infection.

Nervous System

Chronic HCV infection is occasionally associated with a wide range of adverse neurological effects such as inflammatory responses in the brain, cognitive impairment, fatigue and depression [13, 14]. In the NS5A infection network, eight bottlenecks were mapped to various enriched pathways associated with the Nervous system (Table S7a). Six bottlenecks were mapped to the enriched KEGG pathway "Neurotrophin signaling pathway" (p=3.9×10^{-24}), the components of which function in neuronal development and survival. In addition, 5 bottlenecks each were mapped to "Dopaminergic synapse" (p=8.24×10^{-6}) and "Long-term depression" (p=4.99×10^{-4}) and 1 to "Long-term potentiation" (p=0.001). Thus, NS5A interactions with crucial components of the neural machinery associated with development, survival and learning and memory, may play an important role in the development of adverse neurological symptoms that may accompany HCV infection.

Cell growth and death

HCV infection results in the perturbation of the regulators of the host cell cycle and cell cycle arrest prior to mitosis, which plays a major role in HCC [15, 16]. In the NS5A infection network, four bottlenecks (CDK1, GSK3B, PLK1, TP53) were mapped to the enriched KEGG pathway "Cell cycle" (p=1.06×10^{-21}) (Table S7a). Of these, cyclin CDK1 is implicated in cell cycle deregulation in HCV-induced HCC [17]. Among other interactors, CDK6 is aberrantly expressed is various cancers [18]. Therefore, NS5A interactions with CDK1 and CDK6 may contribute to cell cycle deregulation in the HCV-infected cells and their accumulation in the G2/M phase [15] and subsequently, the progression of HCC.

Modulation of apoptosis is an important aspect of HCV pathogenesis. Hepatocyte apoptosis contributes to liver inflammation and fibrosis, whereas the induction of apoptosis in the peripheral blood mononuclear cells (PMBC), such as the T-cells, significantly impairs the clearance of HCV-infected hepatocytes and contributes to viral persistence [19-22]. The

subversion of lipopolysaccharide-mediated hepatocyte apoptosis by NS5A also plays an important role in HCV pathogenesis [23]. Four bottlenecks (AKT1, PIK3R1, TP53, TRAF2) were mapped to the enriched KEGG pathway "Apoptosis" (p=7.86×10^{-12}) (Table S7a), which is consistent with NS5A modulation of host cell death pathways in HCV infection.

Supplementary References

1. Duttweiler, H. M., A highly sensitive and non-lethal beta-galactosidase plate assay for yeast. *Trends Genet* **1996,** 12, (9), 340-1.

2. Kapushesky, M.; Emam, I.; Holloway, E.; Kurnosov, P.; Zorin, A.; Malone, J.; Rustici, G.; Williams, E.; Parkinson, H.; Brazma, A., Gene expression atlas at the European bioinformatics institute. *Nucleic Acids Res* **2010,** 38, (Database issue), D690-8.

3. MacPherson, J. I.; Sidders, B.; Wieland, S.; Zhong, J.; Targett-Adams, P.; Lohmann, V.; Backes, P.; Delpuech-Adams, O.; Chisari, F.; Lewis, M.; Parkinson, T.; Robertson, D. L., An integrated transcriptomic and meta-analysis of hepatoma cells reveals factors that influence susceptibility to HCV infection. *PLoS One* **2011,** 6, (10), e25584.

4. Boguski, M. S.; Lowe, T. M.; Tolstoshev, C. M., dbEST--database for "expressed sequence tags". *Nat Genet* **1993,** 4, (4), 332-3.

5. Uhlen, M.; Oksvold, P.; Fagerberg, L.; Lundberg, E.; Jonasson, K.; Forsberg, M.; Zwahlen, M.; Kampf, C.; Wester, K.; Hober, S.; Wernerus, H.; Bjorling, L.; Ponten, F., Towards a knowledge-based Human Protein Atlas. *Nat Biotechnol* **2010,** 28, (12), 1248-50.

6. Shoemaker, B. A.; Panchenko, A. R., Deciphering protein-protein interactions. Part I. Experimental techniques and databases. *PLoS Comput Biol* **2007,** 3, (3), e42.

7. de Chassey, B.; Navratil, V.; Tafforeau, L.; Hiet, M. S.; Aublin-Gex, A.; Agaugue, S.; Meiffren, G.; Pradezynski, F.; Faria, B. F.; Chantier, T.; Le Breton, M.; Pellet, J.; Davoust, N.; Mangeot, P. E.; Chaboud, A.; Penin, F.; Jacob, Y.; Vidalain, P. O.; Vidal, M.; Andre, P.;

Rabourdin-Combe, C.; Lotteau, V., Hepatitis C virus infection protein network. *Mol Syst Biol* **2008,** 4, 230.

8. Friedel, C. C.; Haas, J., Virus-host interactomes and global models of virus-infected cells. *Trends Microbiol* **2011,** 19, (10), 501-8.

9. Huang, H.; Jedynak, B. M.; Bader, J. S., Where have all the interactions gone? Estimating the coverage of two-hybrid protein interaction maps. *PLoS Comput Biol* **2007,** 3, (11), e214.

10. Fury, W.; Batliwalla, F.; Gregersen, P. K.; Li, W., Overlapping probabilities of top ranking gene lists, hypergeometric distribution, and stringency of gene selection criterion. *Conf Proc IEEE Eng Med Biol Soc* **2006,** 1, 5531-4.

11. Xu, K.; Bezakova, I.; Bunimovich, L.; Yi, S. V., Path lengths in protein-protein interaction networks and biological complexity. *Proteomics* **2011,** 11, (10), 1857-67.

12. Manganelli, P.; Giuliani, N.; Fietta, P.; Mancini, C.; Lazzaretti, M.; Pollini, A.; Quaini, F.; Pedrazzoni, M., OPG/RANKL system imbalance in a case of hepatitis C-associated osteosclerosis: the pathogenetic key? *Clin Rheumatol* **2005,** 24, (3), 296-300.

13. Fletcher, N. F.; McKeating, J. A., Hepatitis C virus and the brain. *J Viral Hepat* **2012,** 19, (5), 301-6.

14. Monaco, S.; Ferrari, S.; Gajofatto, A.; Zanusso, G.; Mariotto, S., HCV-related nervous system disorders. *Clin Dev Immunol* **2012,** 2012, 236148.

15. Kannan, R. P.; Hensley, L. L.; Evers, L. E.; Lemon, S. M.; McGivern, D. R., Hepatitis C virus infection causes cell cycle arrest at the level of initiation of mitosis. *J Virol* **2011,** 85, (16), 7989-8001.

16. Bahnassy, A. A.; Zekri, A. R.; Loutfy, S. A.; Mohamed, W. S.; Moneim, A. A.; Salem, S. E.; Sheta, M. M.; Omar, A.; Al-Zawahry, H., The role of cyclins and cyclin

dependent kinases in development and progression of hepatitis C virus-genotype 4-associated hepatitis and hepatocellular carcinoma. *Exp Mol Pathol* **2011,** 91, (2), 643-52.

17. Zheng, S.; Tansey, W. P.; Hiebert, S. W.; Zhao, Z., Integrative network analysis identifies key genes and pathways in the progression of hepatitis C virus induced hepatocellular carcinoma. *BMC Med Genomics* **2011,** 4, 62.

18. Wang, G.; Zheng, L.; Yu, Z.; Liao, G.; Lu, L.; Xu, R.; Zhao, Z.; Chen, G., Increased cyclin-dependent kinase 6 expression in bladder cancer. *Oncol Lett* **2012,** 4, (1), 43-46.

19. Deng, L.; Adachi, T.; Kitayama, K.; Bungyoku, Y.; Kitazawa, S.; Ishido, S.; Shoji, I.; Hotta, H., Hepatitis C virus infection induces apoptosis through a Bax-triggered, mitochondrion-mediated, caspase 3-dependent pathway. *J Virol* **2008,** 82, (21), 10375-85.

20. Hanafy, S. M.; Shehata, O. H.; Farahat, N. M., Expression of apoptotic markers BCL-2 and Bax in chronic hepatitis C virus patients. *Clin Biochem* **2010,** 43, (13-14), 1112-7.

21. Kondo, Y.; Machida, K.; Liu, H. M.; Ueno, Y.; Kobayashi, K.; Wakita, T.; Shimosegawa, T.; Lai, M. M., Hepatitis C virus infection of T cells inhibits proliferation and enhances fas-mediated apoptosis by down-regulating the expression of CD44 splicing variant 6. *J Infect Dis* **2009,** 199, (5), 726-36.

22. Lim, E. J.; Chin, R.; Angus, P. W.; Torresi, J., Enhanced apoptosis in post-liver transplant hepatitis C: effects of virus and immunosuppressants. *World J Gastroenterol* **2012,** 18, (18), 2172-9.

23. Tamura, R.; Kanda, T.; Imazeki, F.; Wu, S.; Nakamoto, S.; Tanaka, T.; Arai, M.; Fujiwara, K.; Saito, K.; Roger, T.; Wakita, T.; Shirasawa, H.; Yokosuka, O., Hepatitis C Virus nonstructural 5A protein inhibits lipopolysaccharide-mediated apoptosis of hepatocytes by decreasing expression of Toll-like receptor 4. *J Infect Dis* **2011,** 204, (5), 793-801.

Supplementary Table legends

Supplementary Table S1: Y2H assay identified 17 cDNA clones encoding NS5A interacting proteins.

Supplementary Table S2: List of pairwise NS5A-host protein interactions extracted from various publications using a text mining approach combined with manual curation.

Supplementary Table S3: A list of 132 NS5A interactors and their expression in liver.

Supplementary Table S4: The constituents of the NS5A infection network.

Supplementary Table S5a: HCV NS5A infection network: PPI interactions in a tab-delimited format.

Supplementary Table S5b: The high confidence Human protein interactome (HPI) employed in the analysis.

Supplementary Table S6: The NS5A interacting proteins that were identified as bottlenecks in the HPI.

Supplementary Table S7a: Enriched KEGG Pathway associations for the constituents of the HCV NS5A infection network.

Supplementary Table S7b: Enriched CATH structural domain associations for the constituents of the HCV NS5A infection network.

Supplementary Table S7c: Enriched Gene Ontology (GO) Biological Process term associations for the constituents of the HCV NS5A infection network.

Supplementary Table S7d: Enriched Reactome Pathway term associations for the constituents of the HCV NS5A infection network.

Supplementary Table S8a: Enriched KEGG Pathway associations for the NS5A interacting bottlenecks.

Supplementary Table S8b: Enriched Gene Ontology- biological process associations for the NS5A interacting bottlenecks.

Supplementary Table S8c: Enriched Reactome associations for the NS5A interacting bottlenecks.

Supplementary Table S9: Select overlapping functional themes (Enriched KEGG Pathway associations and Gene Ontology- biological process terms) associated with NS5A interacting bottlenecks.